Exciton Fine Structure of CdSe/CdS Nanocrystals Determined by Polarization Microscopy at Room Temperature

Stefano Vezzoli,*,†,‡,# Mathieu Manceau,†,# Godefroy Leménager,†,§ Quentin Glorieux,† Elisabeth Giacobino,† Luigi Carbone,⊥ Massimo De Vittorio,∥ and Alberto Bramati†

†Laboratoire Kastler Brossel, UPMC-Sorbonne Universités, CNRS, ENS-PSL Research University, Collège de France, 4, Place Jussieu Case 74, F-75005 Paris, France, ‡Center for Disruptive Photonic Technology (CDPT), School of Physical and Mathematical Sciences (SPMS), Nanyang Technological University, 21 Nanyang Link, Singapore 637371, Singapore, §Laboratoire de Physique de la Matière Condensée, CNRS - Ecole Polytechnique, UMR 7643, 91128 Palaiseau, France, ⊥CNR NANOTEC-Istituto di Nanotecnologia U.O. Lecce, c/o Polo di Nanotecnologia-Campus Ecotekne, via Monteroni, 73100 Lecce, Italy, and ∥Istituto Italiano di Tecnologia (IIT), Center for Bio-Molecular Nanotechnologies Via Barsanti sn, 73010 Arnesano (Lecce), Italy. #These authors contributed equally to this work.

ABSTRACT We present a method that allows determining the band-edge exciton fine structure of CdSe/CdS dot-in-rods samples based on single particle polarization measurements at room temperature. We model the measured emission polarization of such single particles considering the fine structure properties, the dielectric effect induced by the anisotropic shell, and the measurement configuration. We use this method to characterize the band-edge exciton fine structure splitting of various samples of dot-in-rods. We show that, when the diameter of the CdSe core increases, a transition from a spherical like band-edge exciton symmetry to a rod-like band edge exciton symmetry occurs. This explains the often reported large emission polarization of such particles compared to spherical CdSe/CdS emitters.
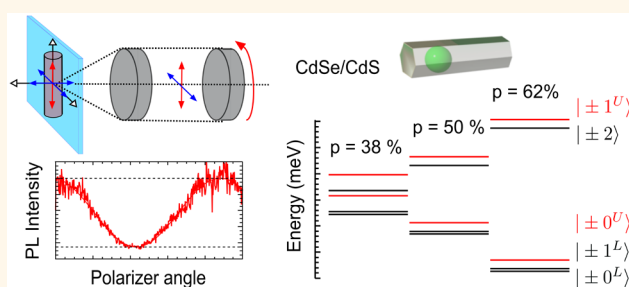
CdSe colloidal nanocrystals are efficient room temperature fluorescent particles. They are used as light emitters in various fields of research such as biological labeling,[1] classical light emitters,[2] and detectors[3] and also for nonclassical light studies.[4−7] The strong confinement of the charge carriers in these nanostructures leads to a fast nonradiative relaxation of multiexcitons[8−12] which results in photon antibunching and single photon emission. This also implies that the emission of such particles is governed only by the radiative relaxation of the band-edge exciton, even at room temperature. The band-edge exciton of CdSe possesses a fine structure[13,14] due to the hexagonal lattice structure of CdSe and to the Coulomb interaction between charge carriers. This structure has been studied with spectroscopic methods at cryogenic temperatures.[15,16]

Among colloidal nanocrystals, nanorods have interesting features as light emitters. In their emission, a high degree of polarization along the wurtzite *c*-axis, which is also the axis of the rod, has been observed and theoretically studied.[17−20] This linearly polarized emission was explained by the fine structure splitting, the levels ordering and the oscillator strengths of the various transitions, which depend on the elongated shape of the nanorods. Due to this shape dependence of level structure, the linear polarization degree grows with the aspect ratio of the nanorod and it is further increased by the anisotropic dielectric environment.[17]

In this paper, we present a study of the polarization emission and of the fine structure of CdSe/CdS dot-in-rods (DRs) made of a spherical core of CdSe surrounded by a rod-like shell of CdS.[21] Conversely to spherical nanocrystals,[22,23] and similarly to
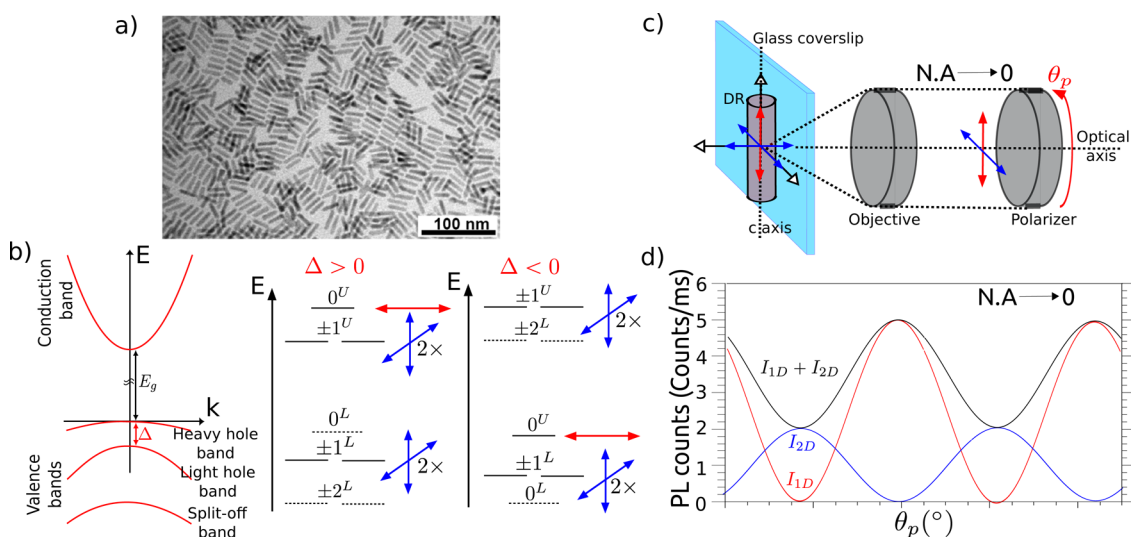
Figure 1. (a) TEM picture of a sample of DRs, showing nanoparticles lying flat onto the support, as well as a good sample homogeneity in the length and diameters of the rod shells (more figures in Supporting Information). (b) Left: Band structure of CdSe, showing the heavy-hole, light-hole and split-off sub-bands and the net-splitting Δ at $k = 0$. Middle: band-edge exciton fine structure energy states for a positive net-splitting Δ. The $|\pm 2\rangle$ states and the $|0^L\rangle$ states are optically inactive and represented as dashed lines. The degenerate 2D dipole emission from $|\pm 1^L\rangle$ and $|\pm 1^U\rangle$ levels is symbolized by the double blue arrows. The 1D dipole emission from $|0^U\rangle$ state is symbolized by the red arrow. Right: band-edge exciton fine structure energy states for negative net-splitting Δ, showing a swapping of the levels. (c) Experimental setup for single particle polarization microscopy. A single DR lies flat on a glass substrate with its c-axis perpendicular to the setup optical axis defined by the objective. A polarizer is placed in the fluorescence path and the measured degree of polarization is determined by the contributions of 1D (red arrows) and 2D dipoles (blue arrows). For an objective with a numerical aperture close to 0, only the field coming from the interface in-plane (plane perpendicular to the optical axis) component of the 2D dipole is collected by the objective. (d) Schematics of a polarization measurement in the case of a numerical aperture close to 0. The measured degree of polarization of the overall emission (black) depends on the mixture of 1D (red) and 2D (blue) contributions.

nanorods, DRs have been reported[5,21,24−26] to show high degrees of emission polarization, typically around 70%. Moreover, they have interesting features as light emitters. They display a strongly reduced emission intermittency (reduced blinking) when synthesized with thick CdS shells,[6] and with a well adjusted geometry they have also be shown to be nearly perfect single photon emitters.[6,27] The situation for DRs is however less clear than for the nanorods mentioned above due to their more complex geometry. In fact, as reported in ref 28, for a specific sample of dot-in-rods, the spherical symmetry of the core should lead to a band-edge exciton structure with the same symmetry as for spherical shell nanocrystals and then to a low polarization degree in the emission. This is in contrast with the observed polarized emission, which seems to indicate that the growth of the anisotropic shell around the core can modify the electronic structure of these particles, as reported for CdSe/CdS dot-in-plates,[29] for example. Further investigations of the structure are thus needed, and this is the subject of this article.

In the following, we show that the study of the emission polarization of the dot-in-rods allows us to retrieve the band-edge exciton fine structure of these emitters at room temperature, without the need of low temperature spectroscopy. First, we present a model of the emission polarization of our DRs taking into account the band-edge exciton fine structure, the shell anisotropy and the measurement configuration and

we show that the degree of polarization at room temperature is strongly correlated with the fine structure. We then present measurements of the emission of single particles with different geometries. On the basis of our model, we deduce the band-edge exciton fine structure characteristics from the polarization measurements for these various dots in rods, and we study their dependence on the shape parameters. We are thus able to explain the difference of polarization between samples with different geometries. Our results also show that the fine structure and the polarization can be widely tuned by changing the geometric parameters of both shell and core, allowing for unprecedented tunability of the optical properties.

RESULTS AND DISCUSSION

Model for the Polarization of the Emitted Light. In this first section, we model the polarization of emission of DRs as a function of the band-edge exciton fine structure, the shell dielectric environment and the measurement configuration.

We first define the degree of emission polarization of a single DR particle and describe the measurement scheme, as it plays a major role in defining the degree of polarization. Polarization measurements are realized on single particles with a broad band linear polarizer (see Figure 1c). For each single DR excited by a laser, the fluorescence is collected by means of a high numerical aperture objective. The resulting photocurrent

measured on an avalanche photodiode is therefore modulated by the polarizer and it can be fitted by the function:

$$I(\theta_p) = (I_{max} - I_{min}) \cos^2(\theta_p) + I_{min} \qquad (1)$$

This is the Malus law for a partially polarized light, whose degree of linear polarization p is given by

$$p = \frac{I_{max} - I_{min}}{I_{max} + I_{min}} \qquad (2)$$

with I_{max} and I_{min} the measured maximum and minimum intensity of the modulated curve. θ_p is the angle of the polarizer.

Concerning the experimental configuration, the orientation of a dipole emitter compared to the optical axis (axis of the microscope) is a fundamental parameter in order to correctly interpret the polarization measurements.[30] A one-dimensional dipole emitting linearly polarized light will show a high degree of polarization if oscillating perpendicularly to the optical axis. However, the measured degree of polarization will decrease if the angle between the optical axis and the dipole decreases. The trend with which it decreases depends on the setup configuration, i.e., on the refractive index of the interfaces and objective numerical aperture. Full calculations are given in the Supporting Information.

If the CdS shell grows without stacking faults, then the wurtzite c-axis of the CdSe core and CdS shell is aligned and corresponds to the long axis of the rod shell. The c-axis of the CdSe core is aligned with the c-axis of the CdS shell because it is the lattice anisotropy of the CdSe core that induces the growth process of the shell along the c-axis.[21,24] Transmission electron microscope (TEM) images suggest that DRs lie flat when drop-casted on a substrate, as evidenced by the size homogeneity in Figure 1a. Images for all the samples studied are presented in Supporting Information. The c-axis is lying flat on the coverslip and is therefore perpendicular to the optical axis of our microscope as depicted in Figure 1c. This working hypothesis is confirmed by a systematic study of defocused images of the emission of single DRs, which are presented in the Supporting Information. In the following, for our model, we will assume that DRs are always aligned with their c-axis perpendicular to the optical axis.

Fine Structure and Polarization. The valence band of CdSe is made of 3 sub-bands, the heavy-hole, light-hole and split-off sub-bands. The energy splitting at $k = 0$ of the heavy-hole and light-hole sub-bands is called the net-splitting Δ. The band-edge exciton fine structure of CdSe nanocrystals consists of eight states,[13] as depicted in Figure 1b: $|\pm2\rangle$, $|\pm1^L\rangle$, $|\pm1^U\rangle$, $|0^L\rangle$, and $|0^U\rangle$. The L and U superscripts, for lower and upper, respectively, distinguish sublevels with the same projection but with different total angular momenta. For spherical

CdSe nanocrystals, the L states have lower energies than the U states, as can be seen in Figure 1b, middle. For CdSe nanorods,[31] it has been shown[17,18] that a level swapping of the fine structure appears for a certain aspect ratio of the nanorods. This is illustrated in Figure 1b right. This can be explained by the band structure of CdSe (see Figure 1b, left), where an inversion of the heavy-hole and light-hole sub-bands energy ordering at $k = 0$ implies a change in the fine structure level ordering.

The $|\pm2\rangle$ states are optically forbidden and do not contribute to the room temperature emission. The $|0^L\rangle$ state has zero oscillator strength and is therefore also optically inactive. Room temperature emission is a mixture of recombinations from the $|0^U\rangle$ state and from the degenerate $|\pm1^L\rangle$, $|\pm1^U\rangle$ states.[13] The $|0^U\rangle$ state is associated with a linear 1D dipole that oscillates along the c-axis of the crystal and emits linearly polarized photons. The $|\pm1^L\rangle$ and $|\pm1^U\rangle$ can be seen as two-dimensional (2D) dipoles, meaning dipoles oscillating inside a plane. Because of the level degeneracy, the emission from these transitions is an incoherent superposition of σ^+ and σ^- components,[22,23,32] and the corresponding dipole is called a degenerate 2D dipole. It is equivalent to two linear dipoles, oscillating perpendicularly and in quadrature. These dipoles are contained into the plane perpendicular to the c-axis of the crystal.[13]

The two types of dipoles and the polarization of their far field emission are shown in Figure 1d. Since the DRs are lying with their c-axis on the substrate, in the limit of an objective with a numerical aperture NA → 0, the objective collects from the 2D transitions a field that is strictly perpendicular to the c-axis, while it collects from the 1D transition a field strictly aligned along the c-axis. As illustrated in Figure 1d, the collected fields from the 1D and 2D dipoles oscillates in perpendicular directions and the degree of polarization depends on their relative strengths. Equation 2 can therefore be written as

$$p_{NA \to 0} = \left| \frac{I_{1D} - I_{2D}}{I_{1D} + I_{2D}} \right| \qquad (3)$$

with I_{1D} the probability of emission of the 1D dipole and I_{2D} the probability of emission from the ensemble of 2D dipoles. Considering a large numerical aperture, we can generalize eq 3 by including the effect of the collection of light coming with a broad angular range:

$$p_{NA} = \left| \frac{p_{1D}I_{1D} - p_{2D}I_{2D}}{I_{1D} + I_{2D}} \right| \qquad (4)$$

As shown in Supporting Information, considering the c-axis lying parallel to the substrate and a NA = 0.95 objective, the correction factors are equal to $p_{1D} = 1$ and $p_{2D} = 0.45$.

Emission Probabilities. To complete our model, we have to determine the emission probabilities of the 1D dipole and 2D dipoles, I_{1D} and I_{2D}. These quantities can be calculated from the theory on CdSe fine structure derived in ref 13. The fine structure energy levels are given in Figure 1b, and their energy, ordering and oscillator strength depend on the two contributions that split the band-edge exciton: the electron−hole exchange interaction η and the net-splitting Δ between the heavy-hole and light-hole valence sub-bands. The electron−hole exchange interaction is the Coulomb interaction between the charge carriers, which depends on the carriers wave functions overlap, and thus on the confinement of the electron and the hole. The net-splitting Δ represents the energy difference between the heavy-hole and light-hole valence sub-bands of the CdSe core as presented in Figure 1b.

Let $N(\eta,\Delta)$ be the population of a state at a given temperature, and $f(\eta,\Delta)$ its oscillator strength. Both quantities are functions of the fine structure splitting parameters η and Δ and can be calculated from ref 13. Then, the probability of emission of a state is $I(\eta,\Delta) = N(\eta,\Delta) f(\eta,\Delta)$. For the 1D emission, we have

$$I_{1D}(\eta, \Delta) = I_{0^U}(\eta, \Delta)$$

$$= N_{0^U}(\eta, \Delta) f_{0^U}(\eta, \Delta) \qquad (5)$$

and for the 2D emission:

$$I_{2D}(\eta, \Delta) = I_{\pm 1^U}(\eta, \Delta) + I_{\pm 1^L}(\eta, \Delta)$$

$$= 2 \times (N_{\pm 1^U}(\eta, \Delta) f_{\pm 1^U}(\eta, \Delta) + N_{\pm 1^L}(\eta, \Delta) f_{\pm 1^L}(\eta, \Delta)) \qquad (6)$$

with a factor of 2 because of the degeneracy of the 2D emission states. Depending on the value of the parameters η and Δ, the oscillator strengths[13] of the different energy levels will be modified as well as their energy and ordering and occupancies as well. Therefore, the measured polarization is a function of the fine structure energy parameters η and Δ.

Dielectric Effect. In addition to the band-edge exciton fine structure, the polarization of the emitted electric field depends on the shell anisotropy. The latter induces a dielectric effect that enhances the electric field oscillating along the long axis (c-axis) of the CdS rod shell. Dielectric effects were theoretically calculated in various articles on colloidal particles[17,29,33] with shape anisotropy. An ellipsoid with axes $a = b < c$ shows an anisotropic response to an electric field. Let us call $f_c = E_c(in)/E_c(out)$ and $f_a = E_a(in)/E_a(out)$ the ratios of electric field amplitudes inside the rod over the electric field amplitude outside the rod, along c and a, respectively, also called local field factors.[33] $R_e = f_c/f_a$, hereafter referred to as the dielectric effect parameter, is the ratio of electric field attenuation between the major and minor axis. In our case $f_c > f_a$ and consequently $R_e > 1$

(see Supporting Information for more information). This implies a stronger attenuation of the electric field in the directions perpendicular to the c-axis. The oscillator strength of a transition along the c-axis should be multiplied by R_e to account for the dielectric shape effect.[17,29] This implies that eq 5 has to be rewritten as

$$I_{1D}(\eta, \Delta, R_e) = I_{0^U}(\eta, \Delta)$$

$$= R_e \times N_{0^U}(\eta, \Delta) f_{0^U}(\eta, \Delta) \qquad (7)$$

Simulations. We now proceed to a theoretical analysis of the degree of polarization p depending on the fine structure energy parameters Δ, η and the dielectric factor R_e.

The heavy-hole light-hole net-splitting Δ has two contributions,[13] the intrinsic splitting Δ_{int} due to the crystal field of the hexagonal lattice structure of CdSe and the shape splitting Δ_{sh} due to possible deviations of the core from a perfect spherical shape. We consider a possible additional contribution for our DRs that we will call the strain splitting Δ_{strain} that has been observed for dot-in-plates.[29] This contribution is due to the strain imposed by the growth of an anisotropic shell around the core that modifies the electronic structure[34] of the core. The net splitting Δ is then:

$$\Delta = \Delta_{int} + \Delta_{sh} + \Delta_{strain} \qquad (8)$$

The intrinsic splitting for CdSe is $\Delta_{int} = 23$ meV. If there is a slight deviation of the core from a perfect sphere, we expect that the core is elongated along the c-axis (prolate), as it is confirmed by TEM images of the core seeds provided in Supporting Information. Moreover, the growth of the CdSe shell could also eventually stretch the core shape along the c-axis. Δ_{sh} is negative in the case of a prolate shape. We also expect a negative contribution from the strain $\Delta_{strain} < 0$. Indeed, for CdSe/CdS dot-in-plates[29] a positive strain contribution to the net-splitting is reported $\Delta_{strain} = +40$ meV because of the growth of the anisotropic CdS shell upon the CdSe core. However, we should be in the opposite case for DRs as the shell growth happens along the c-axis and not in the perpendicular plane as it is the case for dot-in-plates. For our simulations, we have chosen $\Delta \in [-100;23]$ meV.

The electron−hole interaction η depends on the size of the dot for bare CdSe particles. It decreases toward 0 for increasing dot sizes as the electron−hole wave functions overlap decreases.[13] For bare CdSe dots of 2 nm diameter, the smallest core diameter for our samples, calculations[13] gives $\eta = 16$ meV. We therefore take $\eta \in [0;16]$ meV for our simulations.

Using the theory of reference,[13] we calculated the polarization given by eq 4 as a function of the net-splitting Δ and the electron−hole interaction η. Figure 2 shows the results for different values of the dielectric
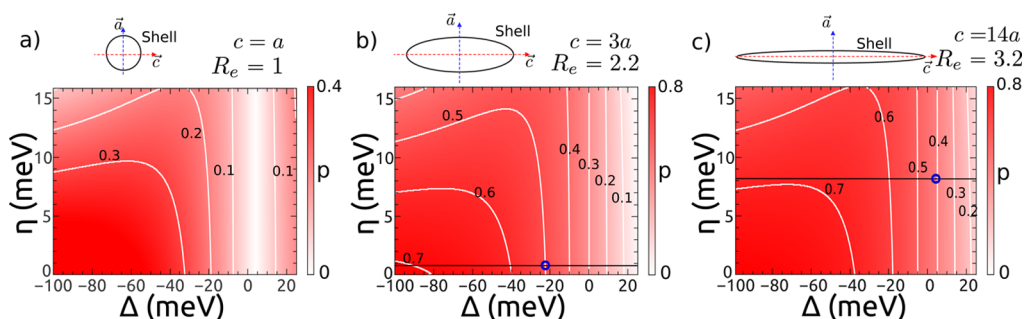
Figure 2. Polarization as a function of the net-splitting Δ and the electron−hole interaction η for different dielectric shape factors R_e. (a) $R_e = 1$: spherical CdS shell. (b) $R_e = 2.2$: CdS rod shell with an aspect ratio of 3.1. This aspect ratio corresponds to sample DR3.1 presented in the following. (c) $R_e = 3.2$: CdS rod shell with an aspect ratio of 14.2. This aspect ratio corresponds to sample DR1 presented in the following. Black horizontal line in (b) and (c) corresponds to the calculated value of electron−hole interaction η for these samples, as described in Supporting Information. The average degree of polarization found for these samples is, respectively, $p = 0.5$ and $p = 0.41$. The corresponding values of net-splitting are $\Delta = -22$ meV and $\Delta = 4.5$ meV. The blue circle represents therefore the coordinates of energy parameters for these samples given their polarization.

TABLE 1. Experimental Data of the Investigated Samples[a]

	core diameter	thickness	length	aspect ratio	R_e	p	Δ
	(nm)	(nm)	(nm)				(meV)
DR1	2	3.6	51	14.2	3.2	0.41 ± 0.13	4.5, [−10.8;15]
DR2	3.3	4	22	5.5	2.8	0.69 ± 0.17	−49, [< −100;−14]
DR3.1	3.3	7	22	3.1	2.2	0.50 ± 0.12	−22, [−46;−7.7]
DR3.3	3.3	7	58	8.3	3	0.65 ± 0.16	−30, [< −100;−7]
DR4	4.6	11	29	2.6	1.9	0.68 ± 0.12	−82, [< −100;−40]

[a] From left to right: geometrical parameters and dielectric effect factor R_e of the investigated samples; average and standard deviation of the distributions of Figure 4, showing the degree of polarization p obtained from measurements over about 40 DRs per sample. The net-splitting Δ is deduced from the measured average values of p and R_e through our theoretical model. The values in square brackets represent the upper and lower values calculated for $p \pm \sigma$. $\Delta = -100$ meV represents the lower bound corresponding to $p_{max} \gtrsim 82\%$ (the precise limit depends on the specific value of R_e). Since for a given value of R_e our model predicts a maximum attainable degree of polarization, our model fails to predict Δ values lower than −100 meV.

shape factor R_e. Figure 2a corresponds to a spherical shell nanocrystal for which no antenna enhancement exists, $R_e = 1$. The patterns in Figure 2b,c are calculated for $R_e = 2.2$ and $R_e = 3.2$, respectively, which correspond to DRs with a moderate shell aspect ratio of 3.1 and a large shell aspect ratio of 14.2. In the next sections, we will present measurements on DR samples having these shell aspect ratios.

First of all, the theory shows that it is not possible to reach high degrees of polarization for spherical shell particles. In Figure 2a, the degree of polarization is limited to a value of 0.4 for high negative values of net-splitting. This can be explained by the fact that the strength of the 1D transition becomes important only with increasing dielectric shape factor R_e. We therefore see that a rod-shape shell is a prerequisite in order to achieve high degrees of polarization, independently of the fine structure energy parameters η and Δ.

The second important consideration is that, for $\eta \lesssim 5$ meV or for $\Delta > 0$, the polarization p depends only on Δ. When we have nanocrystals with a CdS shell, the electron−hole interaction is weaker than in the case of particles without a shell as the electron spreads in the shell.[35] This was experimentally verified in refs 36 and 37 which report values of η lower than 5 meV. For all

these reasons, the contribution of η to the polarization of emission should be negligible in our case.

It is the value of Δ which controls the swapping of levels illustrated in Figure 1b. In Figure 2a, $p = 0$ for $\Delta \simeq 4$ meV when the 2D dipoles and the 1D dipole emission become comparable and cancel each other, due to the swapping of the energy levels. For higher R_e, this swapping happens for larger values of Δ. We can also observe that large negative values of Δ are required to reach a high degree of linear polarization. This corresponds to a fine structure with highly spaced energy levels, as detailed later on. In the following, we show with these calculations that a measurement of polarization gives access to the net splitting Δ and allows for the reconstruction of the fine structure.

Polarization Measurements. We used high quality CdSe/CdS core−shell DRs synthesized using the seeded growth approach proposed in reference.[6,21] In Table 1 we give the core diameter, shell thickness and shell length of the various samples we studied. TEM pictures and optical spectra of both the CdSe seeds and the DR samples are given in Supporting Information. The ratio of electric fields strengths R_e between the major and minor axis for the DRs studied is also given in Table 1 (see Supporting Information for the details
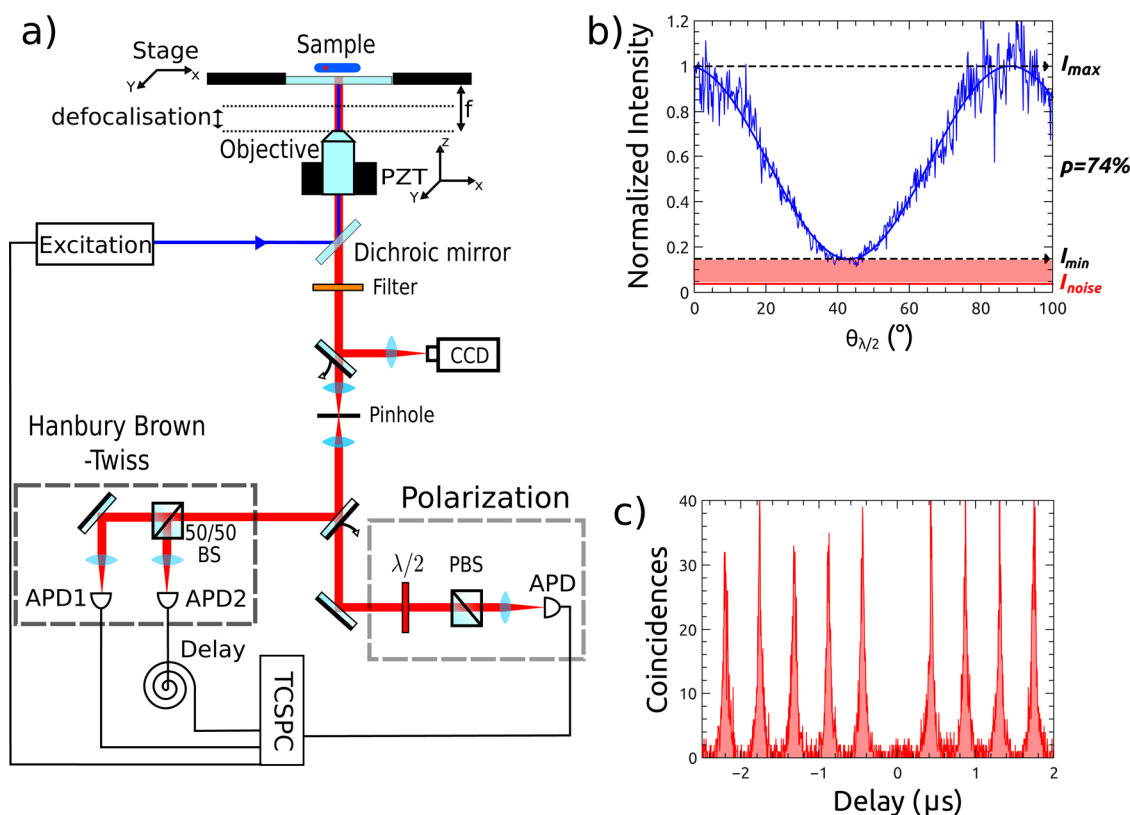
a)

b)

c)

Figure 3. (a) Scheme of the setup for single particle polarization spectroscopy. In a confocal microscope, a single DR is excited using a circularly polarized picosecond pulsed laser diode at 405 nm. The photoluminescence (PL) is collected through an objective and directed either to two single-photon avalanche photodiodes (APD) in a Hanbury-Brown and Twiss configuration, or to a combination of a half-wave plate and a polarizing beam splitter for the analysis of the degree of polarization. (b) An example of single particle polarization measurement. The normalized counts from the APD (blue line) are plotted as a function of the half-wave plate angle. After subtraction of the average background (red line), the curve is fitted by eq 1 to derive the degree of linear polarization. (c) An example of the antibunching test which is performed preliminary to the polarization measurement, in order to check if the chosen particle is single or not. The ratio between the peak at zero delay and the side peaks is proportional to the autocorrelation function at zero delay $g^{(2)}$ (0).

of the calculations). We can see that R_e ranges from 1.9 to 3.2.

A detailed scheme of the experimental setup is presented in Figure 3a. A dilute solution of each DR sample is drop-casted on a glass coverslip to produce a low density distribution of single DRs, which are excited one by one using a circularly polarized 405 nm pulsed laser. After filtering out the laser reflection and the fluorescence from the glass substrate, the photoluminescence (PL) of single DRs is collected using a confocal microscope with a 100×, NA = 0.95 objective. The PL is then sent to two single-photon avalanche photodiodes (APD) in a Hanbury-Brown and Twiss configuration. Preliminary to any polarization measurements, we can check if the chosen particle is single or not with an antibunching measurement, as illustrated in Figure 3c. If the particle is single, the PL is sent to a rotating half-wave plate combined with a polarizing beam splitter to measure the degree of polarization. For each single particle, we plot the number of counts detected by the APDs during a typical time window of 100 ms as a function of the half-wave plate angle, as exemplified in Figure 3b. The noise, mainly

due to the residual fluorescence of the glass substrate, is taken into account and it is subtracted before fitting the intensity curve by eq 1. More details about the experimental setup and the measurement process are provided in the Methods section.

It can be noticed from Figure 3b that the signal is not shot-noise limited, because of the PL fast switching (flickering) between a bright state and a gray, or dark, state with lower emission efficiency. PL flickering and blinking are commonly attributed to a photoinduced charging process.[38] Photo charging can affect the emission polarization; however, it considerably depends on the type of considered nanocrystals and on the excitation conditions. For example, ref 39 reports a similar degree of polarization (within 5%) for the neutral and a charged state with electrons delocalized into the shell, while a significantly lower degree of polarization is found for a different charged state with electrons more localized around the core, although the intensity of this state is also much lower. It must be noted that the DRs in this work were synthesized with a process[24] which is different from ours.[21] In another publication,[40] DRs synthesized with the same method
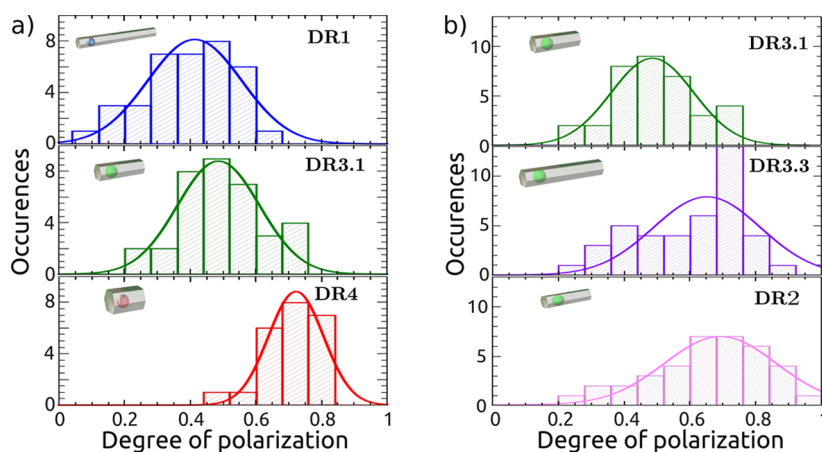
Figure 4. Histogram of the degree of linear polarization. (a) Blue, DR1; green, DR3.1; red, DR4. Different core diameters, lengths, and thicknesses. (b) Green, DR3.1; violet, DR3.3; pink, DR2. Same cores, DR3.1 and DR3.3, same thicknesses and different lengths; DR3.1 and DR2, same length and different thicknesses.

as the one presented here and having similar geometrical parameters always exhibit a degree of polarization of the charged state which is exactly the same as that of the neutral state.

Here, we focus on the fine structure of the neutral state. For this reason, we choose a low pumping power, for which about 0.3−0.5 electron−hole pairs are excited. We demonstrated that for such pumping levels, the percentage of photons coming from the charged state is typically below 10%. Unlike ref 39, in our case only the neutral states and one charged state are present most of the time, as confirmed by an analysis of the lifetimes,[6,27] and the charged state has quantum yield between 30% and 50% of the neutral state. Therefore, the overall measured degree of polarization should be equal or very close to that of the neutral state. Finally, we reject the time traces which show long periods of low intensity, which could be associated with other rare charged states with very low level of polarization. For all these reasons, we can safely conclude that our data reflect the fine structure of the neutral exciton.

Figure 4 shows the histogram of polarization for the different samples studied. The histograms are obtained after measurements of 35−40 nanocrystals per sample. Figure 4a presents samples with different core sizes, while samples with the same core size but different shell lengths and different thicknesses are shown in Figure 4b. Table 1 gives the polarization mean values and standard deviations obtained by fitting the histograms with a Gaussian distribution for every sample. Even if our measurements show large dispersions, it is evident that different samples have different average values of polarization.

It appears that for a given core size, both the shell length and its thickness play a role in defining the degree of polarization as it is clear in Figure 4b: a longer shell increases the degree of polarization while a thicker shell decreases the degree of polarization.

The effect of the core size is illustrated in Figure 4a: in this case all the geometrical parameters are changing, nevertheless we can see that samples with larger cores (in particular DR4) show a higher polarization degree, even though the aspect ratio of the shell is decreasing. It is worth to notice that small cores naturally promote the growth of a thin and long shell. Conversely large cores seed the growth of shell with lower aspect ratios.

For ensemble measurements in solution, we can find in literature average values of emission polarization p of DR samples in the same range of values as for our measurements. References 25 and 41 present measurements on various samples, values of p from 0.5 up to 0.7 are found. The conclusion of ref 41 is that the degree of polarization depends on the ratio of the core diameter over the shell thickness. Our measurements are compatible with this statement when comparing DR2 and DR3.1 that have the same geometrical parameters except their thicknesses. However, in our case the core diameter itself seems to play a major role in defining the polarization, and this fact has never been pointed out in literature before. We can see in Table 1 that DR4 has a small ratio between core diameter and shell thickness compared to DR1, but it has a much higher average polarization degree.

It can be noticed that our measurements show rather large dispersions. Let us point out that the experimental error in the assessment of the degree of polarization is about 5%, mainly attributed to inhomogeneities in the background (we subtract the same average value to all the curves) and to fitting errors, especially for particles with higher flickering of the emission. Ensemble measurements[25,41] show low dispersion, since in this case the polarization is naturally averaged. Single particle measurements with polarization degree ($p = 0.75$) and dispersion comparable to those herein presented (although slightly lower) are reported in the literature.[26] This indicates

that for a given sample the degree of polarization may fluctuate significantly from dot to dot. This is consistent with our finding that the emission polarization is strongly dependent on the details of the fine structure. Small changes of the core shape or different levels of strain between the core and the shell can always be present, even within a sample with a low dispersion (between 5 and 10%) of the geometrical parameters. The core shape and the core/shell strain are precisely the main contributions to the net-splitting Δ in eq 8, which is a decisive parameter to determine the emission polarization p, as illustrated in Figure 2.

Fine Structure. We now use the model presented above and the polarization measurements of different DR samples to estimate their fine structures. By doing so, we elucidate why and how the contributions of the 1D and 2D dipoles to the polarization degree strongly depend on the ordering of the levels and on their spacing, which is mainly given by the net-splitting Δ. Finally, we interpret the dependence of Δ on the geometrical parameters in terms of contributions from the shape of the core Δ_{sh} and from the strain between the core and the shell Δ_{strain}.

From the simulations of Figure 2, for a given R_e and a measured average value of p, we have a set of values of (η, Δ). Let us first consider the case of DR1 shown in Figure 2c. Since the polarization degree is not high, $p < 0.5$, it can be seen that the p value does not depend on η and Δ can be determined easily. For $p = 0.41$, we obtain $\Delta_{DR1} \simeq 4.5$ meV. In all other samples, since the core is larger and the shell thicker, we can consider $\eta \lesssim 1$ meV so that Δ is almost in a one-to-one relation with p, as illustrated in Figure 2b.

We can determine Δ with even higher accuracy, by estimating the value of η from measurements of the dark-bright exciton splitting Δ_{bd} given in literature[37] (refer to Supporting Information for more details). The dark-bright exciton splitting Δ_{db} is the difference of energy between the lowest fine structure level that is always optically inactive ($|\pm2\rangle$ or $|0^L\rangle$) and the first optically active level ($|\pm1^L\rangle$) and it can be measured at cryogenic temperatures. It is related to both Δ and η by the relationship:[13,36,37]

$$\Delta_{db} = E_{\pm1}^L - E_{\pm2}$$
$$= 2\eta + \Delta/2 - \sqrt{(2\eta - \Delta)^2/4 + 3\eta^2} \quad (9)$$

when $\Delta > 0$ and

$$\Delta_{db} = E_{\pm1}^L - E_0^L$$
$$= 2\eta - \Delta/2 - \sqrt{(2\eta - \Delta)^2/4 + 3\eta^2} \quad (10)$$

when $\Delta < 0$. When $|\Delta| \gg \eta$ and $\Delta < 0$, eq 10 shows that η can be approximated as Δ_{db}, and thus it can be estimated from the data given in literature for all the samples for which $\eta \lesssim 1$ meV $\ll |\Delta|$. With the

knowledge of the precise value of η and the measured degree of polarization p, the net-splitting Δ can be determined with better precision. For instance, for DR3.1 one obtains $\eta_{DR3.1} = 0.9$ meV, and therefore, $\Delta_{DR3.1} \simeq -22$ meV from the polarization map in Figure 2b.

For DR1 $\Delta > 0$ and $|\Delta|$ is of the same order as η, so η cannot be approximated as Δ_{db}. However, in this case, the value of the net-splitting is uniquely fixed by the polarization measurement, $\Delta = 4.5$ meV. Therefore, it is still possible to use Δ_{db} to calculate η by using eq 9 without any approximation. In Table 2 we report the values of η and the values of Δ determined from the average degree of polarization measured for each DR sample.

In Table 2 we also give the calculated oscillator strengths and populations of the various levels. We notice that the $|\pm1^L\rangle$ state has a small oscillator strength compared to the other states. To qualitatively understand the polarization properties of the different samples, we can therefore focus the discussion on a comparison between the populations and oscillator strengths of the $|\pm1^U\rangle$ and $|0^U\rangle$ states. Figure 5 shows the calculated energy levels for the different samples using the values of η and Δ from Table 2. The $|\pm1^U\rangle$ and $|0^U\rangle$ levels are highlighted in red. For the specific case of DR3.1, we presented the fine structure levels calculated for the sample average value $p = 0.5$ and for $p \pm \sigma$, being σ the standard deviation of the experimental distribution of p values. This underlines the fact that single particles belonging to the same batch of DRs and sharing similar geometrical parameters can indeed display quite different fine structures.

We can also notice that increasing values of p are associated with the fine structure levels shrinking into two clusters, separated by Δ. Since the $|0^U\rangle$ state lies in the lower energy cluster and the $|\pm1^U\rangle$ state is far above, with an energy difference larger than the thermal energy k_BT, the emission becomes dominated by the 1D dipole for highly negative values of Δ. However, the state $|\pm1^L\rangle$ also lies in the lowest energy group, and even if its 2D dipole contribution is rather small, it sets an upper bound to the maximum achievable level of polarization, according to eq 3. Therefore, our model predicts a maximum achievable degree of polarization $p_{max} \approx 82\%$ (the precise limit depends on the specific value of R_e), which is systematically reached for $\Delta \sim -100$ meV. This implies that the fine structure cannot be inferred from the measurement of the degree of polarization for DRs with $\Delta \sim -100$ meV. This is the reason why for samples DR2, DR3.3 and DR4 the lower limit of Δ cannot be determined and it is arbitrary set to -100 meV, as illustrated in the last column of Table 1. We point out that we experimentally found some particles showing p values slightly higher than p_{max}. This apparent inconsistency can be assigned first to the dispersion of R_e values from particle to

TABLE 2. Fine Structure and Emission Parameters for the Different Samples Investigated, Calculated from the Measured Polarization Mean Values Given in Table 1, the Theoretical Model, and Reference 13[a]

	η (meV)	Δ (meV)	$R_e f_{0^U}$	N_{0^U}	$2f_{\pm 1^L}$	$N_{\pm 1^L}$	$2f_{\pm 1^U}$	$N_{\pm 1^U}$	I_{1D}	I_{2D}
DR1	8.1	4.5	61.7%	17.2%	0.2%	63.2%	38.1%	19.5%	59%	41%
DR2	2.6	−49	58.3%	39.4%	7.6%	54.1%	34.1%	6.5%	78%	22%
DR3.1	0.9	−22	52%	39.1%	9.4%	43.6%	38.6%	17.3%	65.4%	34.6%
DR3.3	0.9	−30	60.4%	41%	8.3%	45.7%	31.3%	13.3%	75.7%	24.3%
DR4	0.3	−82	48.7%	48.1%	12.5%	49.8%	38.7%	2.5%	76.9%	23.1%

[a] From left to right: electron—hole exchange interaction η and net-splitting Δ, oscillator strengths f and populations N of the various emitting levels $|0^U\rangle$, $|\pm 1^L\rangle$ and $|\pm 1^U\rangle$, probability of emission of the 1D dipole I_{1D} and probability of emission from the ensemble of 2D dipoles I_{2D}.
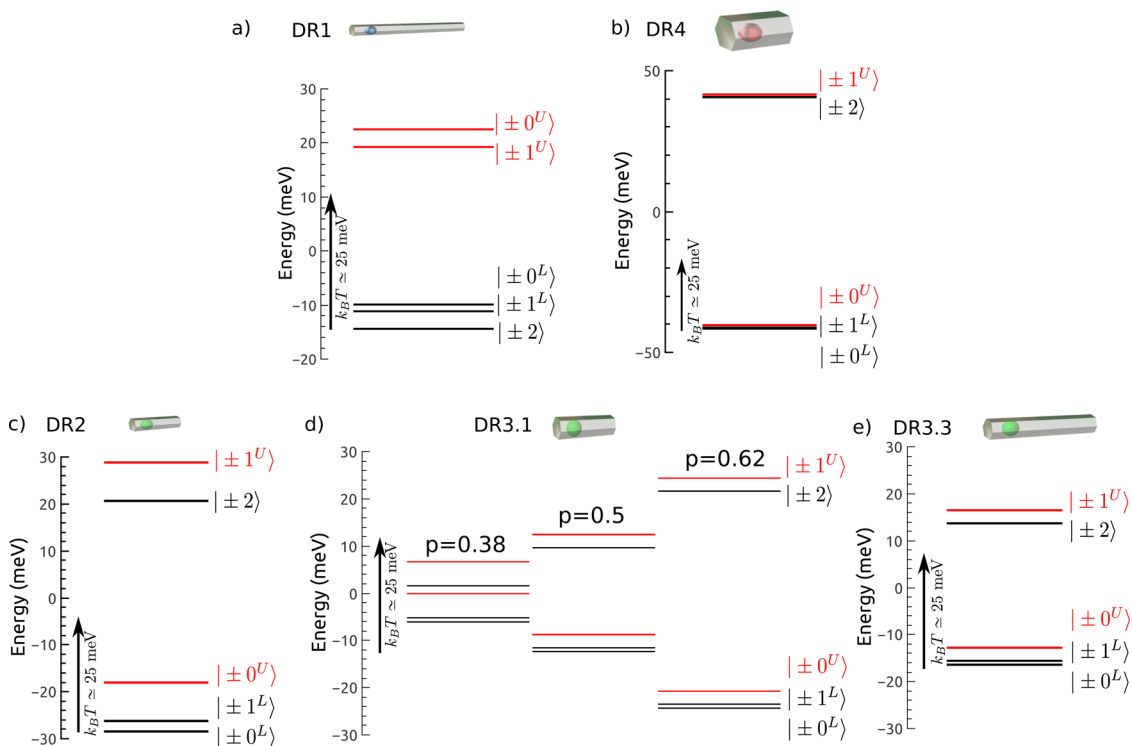

Figure 5. Band edge exciton fine structure deduced from the measured average degree of polarization p and average dielectric factor R_e summarized in Table 1 for samples: (a) DR1, (b) DR4, (c) DR2, (d) DR3.1, and (e) DR3.3. As an example of the effect of the measurement dispersion on the estimation of Δ, we present the fine structure of DR3.1 calculated for the average p plus or minus one standard deviation. The thermal energy at 290 K is 25 meV. It should be noticed that the scale is the same for (c)−(e) but different scales are used for (a) and (b).

particle, whereas p_{max} is calculated from the average value for the sample. Second errors in the estimation of the PL background can easily lead to the overestimation of p, especially for high level of polarization where the minimum of the intensity I_{min} is close to the background level.

Only DR1 displays a spherical-like level ordering ($\Delta > 0$). Despite the large oscillator strength (61.7%) of the 1D dipole of the $|0^U\rangle$ transition (due to the large dielectric effect: $R_e = 3.2$) the polarization is only of 41% for this sample because this state is poorly populated (17.2%) due to the level ordering. For the other samples, the level ordering is different and the $|0^U\rangle$ state has a lower energy than $|\pm 1^U\rangle$ state (see Figure 5). It has therefore a larger population ($\gtrsim 40\%$) and consequently the degree of polarization is higher than for DR1. The samples displaying the largest negative netsplitting Δ, DR2 and DR4, have a lower population (6.5% and 2.5% respectively) for the $|\pm 1^U\rangle$ and thus they display a large polarization degree. This explains why, as can be seen in Figure 2, large negative values of net-splitting Δ are necessary (together with $R_e > 1$) to reach high degree of polarization, because this decreases the emission from the strong 2D transition $|\pm 1^U\rangle$.

Our results thus indicate that there should be a transition between a spherical-like band-edge exciton symmetry to a rod-like (prolate) band-edge exciton symmetry for DRs when increasing the core size from 2 to 3.3 nm. Reference 28 reports a spherical-like bandedge exciton symmetry for DRs with core diameter of $d = 3.2$ nm, shell length $l = 39.8 \pm 1.7$ nm and thickness $t = 4.3 \pm 0.5$ nm. This size is closer to that of DR2 than to

DR1, but the precise size at which the transition happens might depend also on the core seeds and synthesis parameters. In any case, this transition is governed by the change of sign of Δ. Δ decreases toward negative and larger values for larger cores. Moreover, from the comparison between DR3.1, DR3.3 and DR2, we can deduce that $|\Delta|$ increases for thinner and longer shell.

As already stated in eq 8, two phenomena can explain the variations of net-splitting Δ from sample to sample. First, the deviation of the core from a perfect sphere. If the core is elongated along the *c*-axis (prolate), the net-splitting decreases.[13] Second, the growth of the anisotropic shell around the core can induce an anisotropic strain.[29]

DR1 with a very small core, despite its large aspect ratio, has a small and positive net-splitting value (Δ_{DR1} = 4.5 meV), indicating a negligible effect of strain and an almost spherical shape of the core. DR4, which has the largest core, shows the largest value of net-splitting: Δ_{DR4} = −82 meV. The core of this sample must have a strong ellipticity, consistently with other works[41,42] and the TEM images presented in Supporting Information, even if a contribution from strain is also possible. This suggests that both the strain effects and the shape of the core depend on the core diameter. The results for DR2, DR3.1 and DR3.3, showing intermediate values, are consistent with this picture. Moreover, DR2, DR3.1 and DR3.3 have the same core (they were synthesized from the same seeds), so they should have the same ellipticity. Consequently, the net-splittings Δ_{DR2}, $\Delta_{DR3.1}$ and $\Delta_{DR3.3}$ should only differ because of the strain effect Δ_{strain}. From Table 2, we find that Δ_{DR2} = −49 meV, $\Delta_{DR3.1}$ = −22 meV and $\Delta_{DR3.3}$ = −30 meV. Therefore, we can conclude that, for a given core size, the strain increases for thinner and longer shell.

CONCLUSIONS

In this paper, we have presented for the first time a method to determine the fine structure of the band-edge exciton of CdSe/CdS DRs, through measurements of the emission polarization of single particles at room temperature. By modeling the emission as a superposition of contributions from 1D and 2D dipoles, corresponding to different optically active energy levels of the fine structures, we have found a strong correlation between the measured degree of polarization and the splitting of the fine structure levels.

Our study also has the fundamental interest of revealing the physical origin of the different behavior of spherical core−shell nanocrystals and DRs. We have demonstrated that the dielectric effect, despite being necessary to enhance the 1D dipole contribution, cannot alone explain the difference between DR samples, since it is basically omnipresent in all the samples studied. The emission polarization in DRs thus requires a full understanding of the exciton fine structure. By studying different samples, the effect of the relevant geometrical parameters—core size and shell thickness and length —on the emission polarization, and thus on the fine structure, has been elucidated. We find that an increasing size of the core causes a swapping of the energy levels respectively responsible for the 1D and the 2D dipole emission. This is a primary requirement to reach a high degree of linear polarization, and we demonstrated that this is caused by a change of the core shape with the dimension. A thin and long shell can further enhance the degree of polarization, by acting on the spacing between the levels through a strain effect between the core and the shell.

Apart from the fundamental interest, our work represents a step toward a better control and engineering of the optical properties of CdSe/CdS DRs which are strongly dependent on their fine structure, such as the emission polarization or the lifetime. A fine-tuning of these properties, through a suitable choice of the nanocrystal geometrical parameters, as exemplified in the present work, is crucial in nanophotonics applications such as coupling of single quantum emitter to nano- and microcavities, nanolasers or nanospasers.

METHODS

Synthesis of CdSe/Cds Dot-in-Rod Samples. All syntheses are carried out under air-free conditions using a standard Schlenk line setup. All chemicals are used as received and all solvents used are anhydrous and of analytical grade.

Synthesis of CdSe Nanodots. A total of 3.700 g of trioctylphosphine oxide (TOPO 99% from STREM), 0.280 g of octadecylphosphonic acid (ODPA 99%, Polycarbon Industries), and 0.060 g of cadmium oxide (CdO 99.99%, Sigma-Aldrich) are stirred in a 50 mL flask, heated to 150 °C and exposed to vacuum for 1 h. Afterward, the solution is heated to 300 °C while flushing the flask with N_2 until it turns transparent and colorless. At this point, the growth temperature is set to 370 °C and 1.5 g of trioctylphosphine (TOP 99%, STREM) is injected. After the temperature has recovered the set value, a selenium-TOP solution (0.063 g Se, 100 mesh 99.5%, Sigma-Aldrich + 0.575 g TOP) is at-once injected and the growth is allowed to proceed for 10 s for the seeds of sample DR1 (see Figure S1a in the Supporting Information); 1 min for the seeds of samples DR2, DR3.1, and DR3.3 (see Figure S1b); and 2.30 min for the seeds of sample DR4 (see Figure S1c) before definitely removing the heating mantle. Each CdSe nanodot solution is then transferred into a drybox and twice purified by sequential precipitation and resolubilization with methanol and anhydrous toluene, respectively. Finally, the nanodots are dissolved in TOP in a final CdSe dots concentration of 7.5×10^{-4} M (calculated according to ref 43). See Figure S1 for band-edge absorption, photoluminescence details and TEM analysis.

Synthesis of CdSe/CdS Dot-in-Rods. All synthesis of core/shell CdSe/CdS dot-in-rods were carried out under N_2 atmosphere using a seeded-growth approach elsewhere described.[6,21] In a typical synthetic stage, 0.085 g of CdO is mixed up in a flask with 3.000 g of TOPO, 0.285 g of ODPA and 0.080 g of hexylphosphonic acid (HPA 99%, Polycarbon Industries). The flask is pumped to vacuum for almost 1 h at 150 °C and then, under inert gas flow, the solution is heated separately to 350 °C in the

case of samples DR1, DR2, DR3.1, DR3.3 (see Figure S2 in Supporting Information) or to 360 °C in the case of DR4 (see Figure S2. At this point, 1.5 g of TOP is injected. After the temperature has newly gained the set value, a solution of S precursor-TOP-CdSe nanodots is swiftly injected into the flask. This solution is prepared by dissolving 0.120 g of sulfur (S 99.998%, Sigma-Aldrich) in 1.5 g of TOP and adding 100 μL of a solution of CdSe dots dissolved in TOP (7.5×10^{-4} M). The three different solutions of CdSe nanodots described in the previous paragraph were employed to produce different DR samples. After the injection, the dark red CdSe/CdS nanocrystal solution is allowed to grow respectively for 8 min in the case of sample DR1, DR2, DR4, and 20 min for sample DR3.1. The reaction is then stopped by removing the heating mantle. When the solution temperature cools down to about 70 °C, the nanoparticles are transferred into a glovebox and twice purified by precipitation with anhydrous methanol and resolubilization in anhydrous toluene thus producing CdSe/CdS dot-in-rod solutions diluted to a concentration of 10^{-10} M. In the case of sample DR3.3, after the injection of the S-TOP-CdSe dots solution, the system is left to grow for 15 min, then a $Cd^{2+}-$and $S^{2-}-$rich stock solution dropwise is injected at rate 300 μL/min. After the injection, the system is again left to grow for further 10 min before definitely interrupting the reaction. The whole nanocrystals growth time results to be 40 min. To prepare the $Cd^{2+}-$and $S^{2-}-$rich stock solution, 0.180 g of CdO, 0.850 g of ODPA, 0.250 g of HPA and 3.000 g of TOPO are stirred in a 50 mL flask, heated to 150 °C and exposed to vacuum for 1 h. Afterward, the solution is heated to 300 °C while flushing the flask with N_2 until it turns transparent and colorless. The reaction is then stopped and the solution left to reach the room temperature. To this mixture, a second solution prepared by dissolving 0.360 g of S in 8.5 g of TOP is added at room temperature.

Optical and Morphological Characterization. Absorption measurements were carried out using a Cary 5000 UV–vis spectrophotometer, whereas photoluminescence spectra were recorded in cuvette by using a Cary Eclipse fluorescence spectrophotometer. Low-magnification transmission electron microscopy (TEM) analysis was performed on a Jeol JEM-1011 electron microscope operating at 100 kV, equipped with a CCD camera ORIUS 831 from Gatan. TEM samples were prepared by dropcasting toluene-diluted nanocomposite solutions onto carbon coated copper grids. Afterward, the deposited samples were allowed to completely dry at 60 °C for one night before examination. See Figure S2 in Supporting Information for band-edge absorption and photoluminescence details and TEM analysis.

Single Particle Polarization Microscopy. A detailed scheme of the experimental setup for single particle polarization microscopy is presented in Figure 3a. For each sample, a dilute solution is drop-casted on a microscope glass coverslip to produce a low density of single DRs (2 to 5 DRs per 5 μm^2 area) . A single DR can be chosen and excited using a picosecond (ps) pulsed laser diode with a small excitation spot of 1 μm^2. The ps pulsed laser operates at a wavelength of 405 nm to excite the highly absorptive shell[21] and it is circularly polarized, which ensures a reproducible efficiency of the excitation. The photoluminescence (PL) is collected using a confocal microscope with a high numerical aperture objective (100× NA = 0.95) mounted on a piezoelectric, after filtering out the laser reflection and the fluorescence from the glass substrate by means of a combination of a spectral long-pass filter and of a pinhole, acting as a spatial filter. The PL is then sent to two single-photon avalanche photodiodes (APD) in a Hanbury-Brown and Twiss configuration. The signals from the photodiodes are recorded by a Time-Correlated Single Photon Counting (TCSPC) data acquisition card triggered by each laser pulse, enabling the recording of the PL autocorrelation function for each DR. After the antibunching test, the PL is sent to a rotating half-wave plate combined with a polarizing beam splitter to measure the degree of polarization. We verify that the optical system does not introduce any polarization bias, by sending a linearly polarized laser beam at 633 nm through the same optical path followed by the light emitted by the single nanocrystals.

REFERENCES AND NOTES

1. Wu, X.; Liu, H.; Liu, J.; Haley, K. N.; Treadway, J. A.; Larson, J. P.; Ge, N.; Peale, F.; Bruchez, M. P. Immunofluorescent Labeling of Cancer Marker Her2 and Other Cellular Targets with Semiconductor Quantum Dots. *Nat. Biotechnol.* **2002**, *21*, 41–46.

2. Klimov, V.; Mikhailovsky, A.; Xu, S.; Malko, A.; Hollingsworth, J.; Leatherdale, C.; Eisler, H.-J.; Bawendi, M. Optical Gain and Stimulated Emission in Nanocrystal Quantum Dots. *Science* **2000**, *290*, 314–317.

3. Oertel, D. C.; Bawendi, M. G.; Arango, A. C.; Bulović, V. Photodetectors Based on Treated CdSe Quantum-Dot Films. *Appl. Phys. Lett.* **2005**, *87*, 213505.

4. Lounis, B.; Bechtel, H.; Gerion, D.; Alivisatos, P.; Moerner, W. Photon Antibunching in Single CdSe/ZnS Quantum Dot Fluorescence. *Chem. Phys. Lett.* **2000**, *329*, 399–404.

5. Pisanello, F.; Martiradonna, L.; Leménager, G.; Spinicelli, P.; Fiore, A.; Manna, L.; Hermier, J.-P.; Cingolani, R.; Giacobino, E.; Vittorio, M. D.; et al. Room Temperature-Dipolelike Single Photon Source with a Colloidal Dot-in-Rod. *Appl. Phys. Lett.* **2010**, *96*, 033101.

6. Pisanello, F.; Leménager, G.; Martiradonna, L.; Carbone, L.; Vezzoli, S.; Desfonds, P.; Cozzoli, P. D.; Hermier, J.-P.; Giacobino, E.; Cingolani, R.; et al. Non-Blinking Single-Photon Generation with Anisotropic Colloidal Nanocrystals: Towards Room-Temperature, Efficient, Colloidal Quantum Sources. *Adv. Mater.* **2013**, *25*, 1974–1980.

7. Shcherbina, O. A.; Shcherbina, G. A.; Manceau, M.; Vezzoli, S.; Carbone, L.; Vittorio, M. D.; Bramati, A.; Giacobino, E.; Chekhova, M. V.; Leuchs, G. Photon Correlations for Colloidal Nanocrystals and Their Clusters. *Opt. Lett.* **2014**, *39*, 1791–1794.

8. Efros, A. L.; Kharchenko, V.; Rosen, M. Breaking the Phonon Bottleneck in Nanometer Quantum Dots: Role of Auger-like Processes. *Solid State Commun.* **1995**, *93*, 281–284.

9. Woggon, U.; Giessen, H.; Gindele, F.; Wind, O.; Fluegel, B.; Peyghambarian, N. Ultrafast Energy Relaxation in Quantum Dots. *Phys. Rev. B: Condens. Matter Mater. Phys.* **1996**, *54*, 17681.

10. Klimov, V. I.; McBranch, D. W. Femtosecond 1 P-to-1 S Electron Relaxation in Strongly Confined Semiconductor Nanocrystals. *Phys. Rev. Lett.* **1998**, *80*, 4028.

11. Guyot-Sionnest, P.; Shim, M.; Matranga, C.; Hines, M. Intraband Relaxation in CdSe Quantum Dots. *Phys. Rev. B: Condens. Matter Mater. Phys.* **1999**, *60*, R2181.

12. Hendry, E.; Koeberg, M.; Wang, F.; Zhang, H.; Donega, C. d. M.; Vanmaekelbergh, D.; Bonn, M. Direct Observation of Electron-to-hole Energy Transfer in CdSe Quantum Dots. *Phys. Rev. Lett.* **2006**, *96*, 057408.

13. Efros, A. L.; Rosen, M.; Kuno, M.; Nirmal, M.; Norris, D.; Bawendi, M. Band-edge Exciton in Quantum Dots of Semiconductors with a Degenerate Valence Band: Dark and Bright Exciton States. *Phys. Rev. B: Condens. Matter Mater. Phys.* **1996**, *54*, 4843.

14. Norris, D.; Efros, A. L.; Rosen, M.; Bawendi, M. Size Dependence of Exciton Fine Structure in CdSe Quantum Dots. *Phys. Rev. B: Condens. Matter Mater. Phys.* **1996**, *53*, 16347.

15. Biadala, L.; Louyer, Y.; Tamarat, P.; Lounis, B. Band-edge Exciton Fine Structure of Single CdSe/ZnS Nanocrystals in External Magnetic Fields. *Phys. Rev. Lett.* **2010**, *105*, 157402.

16. Fernée, M. J.; Tamarat, P.; Lounis, B. Cryogenic Single-nanocrystal Spectroscopy: Reading the Spectral Fingerprint of Individual CdSe Quantum Dots. *J. Phys. Chem. Lett.* **2013**, *4*, 609–618.

17. Shabaev, A.; Efros, A. L. 1D Exciton Spectroscopy of Semiconductor Nanorods. *Nano Lett.* **2004**, *4*, 1821–1825.

18. Le Thomas, N.; Herz, E.; Schöps, O.; Woggon, U.; Artemyev, M. Exciton Fine Structure in Single CdSe Nanorods. *Phys. Rev. Lett.* **2005**, *94*, 016803.

19. Louyer, Y.; Biadala, L.; Trebbia, J.-B.; Fernée, M.; Tamarat, P.; Lounis, B. Efficient Biexciton Emission in Elongated CdSe/ZnS Nanocrystals. *Nano Lett.* **2011**, *11*, 4370–4375.

20. Fernee, M. J.; Sinito, C.; Tamarat, P.; Lounis, B. State Selective Pumping Reveals Spin-Relaxation Pathways in CdSe Quantum Dots. *Nano Lett.* **2014**, *14*, 4480.

21. Carbone, L.; Nobile, C.; De Giorgi, M.; Sala, F. D.; Morello, G.; Pompa, P.; Hytch, M.; Snoeck, E.; Fiore, A.; Franchini, I. R.; et al. Synthesis and Micrometer-Scale Assembly of Colloidal CdSe/CdS Nanorods Prepared by a Seeded Growth Approach. *Nano Lett.* **2007**, *7*, 2942–2950.

22. Empedocles, S.; Neuhauser, R.; Bawendi, M. Three-dimensional Orientation Measurements of Symmetric Single Chromophores Using Polarization Microscopy. *Nature* **1999**, *399*, 126–130.

23. Chung, I.; Shimizu, K. T.; Bawendi, M. G. Room Temperature Measurements of the 3D Orientation of Single CdSe Quantum Dots Using Polarization Microscopy. *Proc. Natl. Acad. Sci. U. S. A.* **2003**, *100*, 405–408.

24. Talapin, D. V.; Koeppe, R.; Götzinger, S.; Kornowski, A.; Lupton, J. M.; Rogach, A. L.; Benson, O.; Feldmann, J.; Weller, H. Highly Emissive Colloidal CdSe/CdS Heterostructures of Mixed Dimensionality. *Nano Lett.* **2003**, *3*, 1677–1681.

25. Sitt, A.; Salant, A.; Menagen, G.; Banin, U. Highly Emissive Nano Rod-in-Rod Heterostructures with Strong Linear Polarization. *Nano Lett.* **2011**, *11*, 2054–2060.

26. Hadar, I.; Hitin, G. B.; Sitt, A.; Faust, A.; Banin, U. Polarization Properties of Semiconductor Nanorod Heterostructures: From Single Particles to the Ensemble. *J. Phys. Chem. Lett.* **2013**, *4*, 502–507.

27. Manceau, M.; Vezzoli, S.; Glorieux, Q.; Pisanello, F.; Giacobino, E.; Carbone, L.; Vittorio, M. D.; Bramati, A. Effect of Charging on CdSe/CdS Dot-in-Rods Single-photon Emission. *Phys. Rev. B: Condens. Matter Mater. Phys.* **2014**, *90*, 035311.

28. Granados del Aguila, A.; Jha, B.; Pietra, F.; Groeneveld, E.; Donegá, C. d. M.; Maan, J. C.; Vanmaekelbergh, D.; Christianen, P. C. Observation of the Full Exciton and Phonon Fine-Structure in CdSe/CdS Dot-in-Rod Hetero-nanocrystals. *ACS Nano* **2014**, *8*, 5921.

29. Cassette, E.; Mahler, B.; Guigner, J.-M.; Patriarche, G.; Dubertret, B.; Pons, T. Colloidal CdSe/CdS Dot-in-Plate Nanocrystals with 2D-Polarized Emission. *ACS Nano* **2012**, *6*, 6741–6750.

30. Lethiec, C.; Laverdant, J.; Vallon, H.; Javaux, C.; Dubertret, B.; Frigerio, J.-M.; Schwob, C.; Coolen, L.; Maître, A. Measurement of Three-Dimensional Dipole Orientation of a Single Fluorescent Nanoemitter by Emission Polarization Analysis. *Phys. Rev. X* **2014**, *4*, 021037.

31. Hu, J.; Li, L.-s.; Yang, W.; Manna, L.; Wang, L.-w.; Alivisatos, A. P. Linearly Polarized Emission from Colloidal Semiconductor Quantum Rods. *Science* **2001**, *292*, 2060–2063.

32. Brokmann, X.; Ehrensperger, M.-V.; Hermier, J.-P.; Triller, A.; Dahan, M. Orientational Imaging and Tracking of Single CdSe Nanocrystals by Defocused Microscopy. *Chem. Phys. Lett.* **2005**, *406*, 210–214.

33. Kamal, J. S.; Gomes, R.; Hens, Z.; Karvar, M.; Neyts, K.; Compernolle, S.; Vanhaecke, F. Direct Determination of Absorption Anisotropy in Colloidal Quantum Rods. *Phys. Rev. B: Condens. Matter Mater. Phys.* **2012**, *85*, 035126.

34. Chuang, S.; Chang, C. k.p Method for Strained Wurtzite Semiconductors. *Phys. Rev. B: Condens. Matter Mater. Phys.* **1996**, *54*, 2491.

35. Grazia Lupo, M.; Scotognella, F.; Zavelani-Rossi, M.; Lanzani, G.; Manna, L.; Tassone, F. Band-edge Ultrafast Pump-probe Spectroscopy of Core/shell CdSe/CdS Rods: Assessing Electron Delocalization by Effective Mass Calculations. *Phys. Chem. Chem. Phys.* **2012**, *14*, 7420–7426.

36. Brovelli, S.; Schaller, R.; Crooker, S.; Garcia-Santamaria, F.; Chen, Y.; Viswanatha, R.; Hollingsworth, J.; Htoon, H.; Klimov, V. Nano-Engineered Electron-hole Exchange Interaction Controls Exciton Dynamics in Core-shell Semiconductor Nanocrystals. *Nat. Commun.* **2011**, *2*, 280.

37. Biadala, L.; Siebers, B.; Gomes, R.; Hens, Z.; Yakovlev, D. R.; Bayer, M. Tuning Energy Splitting and Recombination Dynamics of Dark and Bright Excitons in CdSe/CdS Dot-in-Rod Colloidal Nanostructures. *J. Phys. Chem. C* **2014**, *118*, 22309–22316.

38. Cordones, A. A.; Leone, S. R. Mechanisms for Charge Trapping in Single Semiconductor Nanocrystals Probed by Fluorescence Blinking. *Chem. Soc. Rev.* **2013**, *42*, 3209–3221.

39. Ihara, T.; Sato, R.; Teranishi, T.; Kanemitsu, Y. Delocalized and Localized Charged Excitons in Single CdSe/CdS Dot-in-Rods Revealed by Polarized Photoluminescence Blinking. *Phys. Rev. B: Condens. Matter Mater. Phys.* **2014**, *90*, 035309.

40. Lethiec, C.; Pisanello, F.; Carbone, L.; Bramati, A.; Coolen, L.; Maître, A. Polarimetry-Based Analysis of Dipolar Transitions of Single Colloidal CdSe/CdS Dot-in-Rods. *New J. Phys.* **2014**, *16*, 093014.

41. Diroll, B. T.; Koschitzky, A.; Murray, C. B. Tunable Optical Anisotropy of Seeded CdSe/CdS Nanorods. *J. Phys. Chem. Lett.* **2014**, *5*, 85–91.

42. Murray, C.; Norris, D. J.; Bawendi, M. G. Synthesis and Characterization of Nearly Monodisperse CdE (E= Sulfur, Selenium, Tellurium) Semiconductor Nanocrystallites. *J. Am. Chem. Soc.* **1993**, *115*, 8706–8715.

43. Yu, W. W.; Qu, L.; Guo, W.; Peng, X. Experimental Determination of the Extinction Coefficient of CdTe, CdSe, and CdS Nanocrystals. *Chem. Mater.* **2003**, *15*, 2854–2860.